

Canine Distemper Virus Uses both the Anterograde and the Hematogenous Pathway for Neuroinvasion

Penny A. Rudd,¹ Roberto Cattaneo,² and Veronika von Messling^{1*}

INRS-Institut Armand-Frappier, University of Quebec, Laval, Quebec, Canada,¹ and Virology and Gene Therapy Graduate Track, Mayo Clinic College of Medicine, Rochester, Minnesota²

Received 19 May 2006/Accepted 11 July 2006

Canine distemper virus (CDV), a member of the *Morbillivirus* genus that also includes measles virus, frequently causes neurologic complications, but the routes and timing of CDV invasion of the central nervous system (CNS) are poorly understood. To characterize these events, we cloned and sequenced the genome of a neurovirulent CDV (strain A75/17) and produced an infectious cDNA that expresses the green fluorescent protein. This virus fully retained its virulence in ferrets: the course and signs of disease were equivalent to those of the parental isolate. We observed CNS invasion through two distinct pathways: anterogradely via the olfactory nerve and hematogenously through the choroid plexus and cerebral blood vessels. CNS invasion only occurred after massive infection of the lymphatic system and spread to the epithelial cells throughout the body. While at early time points, mostly immune and endothelial cells were infected, the virus later spread to glial cells and neurons. Together, the results suggest similarities in the timing, target cells, and CNS invasion routes of CDV, members of the *Morbillivirus* genus, and even other neurovirulent paramyxoviruses like Nipah and mumps viruses.

Canine distemper virus (CDV) and the closely related viruses that infect marine mammals have the highest incidence of central nervous system (CNS) complications among viruses of the genus *Morbillivirus*. Up to 30% of dogs exhibit signs of neurologic involvement during or after CDV infection, and most wild carnivores that succumb to CDV have some evidence of CNS infection (8, 18, 20, 38, 51). With 1 in 1,000 cases, the neurovirulent potential of measles virus (MV) is comparatively lower, but CNS complications remain one of the main problems associated with MV infections in countries with an established health care system (32). Because of its relatively high degree of neurovirulence and the availability of a sensitive small animal model, CDV is an ideal candidate to characterize the events involved in morbillivirus neuroinvasion.

All morbilliviruses display a strong lymphotropism, which correlates with the presence of their principal receptor, the signaling lymphocytic activation molecule (SLAM, CD150), on a variety of immune cells (6, 36, 40). In ferrets infected with a virulent CDV strain, more than 50% of circulating peripheral blood mononuclear cells (PBMC) contain infectious virus, and up to 10% of PBMC in MV-infected monkeys are virus positive (46, 53). Because of these findings and the fact that morbilliviruses are highly cell associated, it is thought that the contact between virus and CNS occurs through infected PBMC. Previous studies of typical wild-type isolates like strain A75/17 in dogs further support this theory (38).

At the onset of the symptomatic disease around 14 days after intranasal inoculation, infected cells are predominantly detected in the perivascular spaces of the CNS, the choroid plexus, and the ependyma (19, 39). Around 3 weeks after

infection, CDV-positive glial cells and neurons are found in the white matter, and the beginning of demyelination is observed in these regions (41). The CNS infection peaks 4 to 5 weeks after inoculation, when virus is detected in neurons and glial cells throughout white and gray matter in a focal fashion (23, 45, 52). Around 10% of dogs die at this time from acute encephalitis developing while their immune system fails to control the infection.

In animals that mount an effective cellular and humoral immune response, perivascular cuffing and lymphocyte infiltration of the infected areas occur at the same time as the rash and other signs of disease recede, and CDV-specific neutralizing antibodies are detected in the serum and cerebrospinal fluid (CSF) (39, 41, 52). This immune response results in virus clearance from the CNS, but can be accompanied by continued demyelination, which is ultimately responsible for the development of neurological signs in a subset of animals several weeks after recovery from the acute infection (38, 44).

Despite this body of knowledge, the timing and sequence of events during the acute phase of morbillivirus CNS invasion remain unclear, principally because only a fraction of experimentally infected dogs develop acute encephalitis (38, 51) and the available rodent models require injection of the virus into the brain to cause infection (10, 22). We have previously established a morbillivirus pathogenesis model based on the study of CDV in ferrets, one of its natural hosts (46, 47). CDV-infected ferrets develop an acute disease that is usually lethal within 2 to 5 weeks, and there is little variation between animals infected with the same strain (37, 47).

To expand our ferret model to the characterization of morbillivirus neuroinvasion, we first confirmed the neurovirulent potential of A75/17 in ferrets. This strain is a typical representative of canine street isolates that has been extensively characterized in dogs (38). We generated an infectious cDNA clone of this strain, which corresponded exactly to the se-

* Corresponding author. Mailing address: INRS-Institut Armand-Frappier, University of Quebec, 531, Boul. des Prairies, Laval, Quebec H7V 1B7, Canada. Phone: (450) 687-5010. Fax: (450) 686-5305. E-mail: veronika.vonmessling@iaf.inrs.ca.

quence deposited in GenBank (accession no. AF164967), and introduced the reporter gene coding for enhanced green fluorescent protein (EGFP) in this cDNA. The resulting virus facilitated monitoring the CNS invasion routes. We show that CNS invasion occurs only after extensive spread to epithelia. We demonstrate anterograde invasion via the olfactory bulb in addition to the previously characterized hematogenous spread through the choroid plexus and cerebral blood vessels (19). This work directly visualizes, for the first time, different stages of morbillivirus neuroinvasion during the acute disease phase, providing new insights into the disease progression and cellular targets.

MATERIALS AND METHODS

Cells and viruses. VerodogSLAMtag cells (47) and 293 cells (ATCC CRL-1573) were maintained in Dulbecco's modified Eagle's medium (Invitrogen, Burlington, Ontario, Canada) with 5% fetal calf serum (Invitrogen, Burlington, Ontario, Canada). Zeocin (Invitrogen, Burlington, Ontario, Canada) was added (1 mg/ml) to the VerodogSLAMtag cells to maintain the constitutive expression of canine SLAM. All viruses were propagated in VerodogSLAMtag cells. A lymph node homogenate of a dog experimentally infected with CDV strain A75/17 was a kind gift of Max Appel.

Construction and recovery of recombinant viruses. To generate an infectious cDNA clone of the neurovirulent CDV strain A75/17, RNA was isolated directly from the lymph node homogenate. The cloning strategy was the same as those used previously for other CDV vaccine and wild-type strains (47). Briefly, the RNA was reverse transcribed using Superscript II (Invitrogen, Burlington, Ontario, Canada), and the entire genome was amplified in 10 fragments using high-fidelity polymerase (Roche Diagnostics, Laval, Quebec, Canada) and subcloned into pCR-TOPO (Invitrogen, Burlington, Ontario, Canada). At least four clones of each fragment were sequenced to establish a consensus sequence. The viral cDNA clone was then assembled from fragments corresponding to the consensus sequence using naturally occurring unique restriction sites, yielding pA75/17. An EGFP-expressing derivative containing the EGFP open reading frame in an additional transcription unit between the H and L genes (pA75/17eH) was obtained following the cloning strategy for 5804PeH (46). The corresponding recombinant viruses were recovered as described previously, using an MVA-T7-based system (48).

Animal infection, grading of clinical signs, and imaging. The animal experiments were carried out as described previously (47). Briefly, unvaccinated male ferrets (*Mustela putorius furo*) 16 weeks and older (Marshall Farms, North Rose, NY) were then infected intranasally with 10^4 50% tissue culture infectious doses (TCID₅₀) of the respective virus under general anesthesia (10 mg/kg ketamine, 1 mg/kg midazolam; CDMV, St. Hyacinthe, Quebec, Canada). Following the infection, animals were monitored daily for signs of disease, and blood was collected at various time points from the jugular vein under general anesthesia.

A grading system was established to evaluate the severity of clinical signs and to determine end points for the removal of animals from the study. Animals that failed to eat for more than 48 h, experienced weight loss of 15 to 20%, became severely dehydrated, developed CNS signs (circling behavior, paralysis, or focal or generalized seizures), displayed any other important reduction in functional status (severe pneumonia and/or diarrhea), or became moribund before the end of the protocol were euthanized with an overdose of pentobarbital (Nembutal; CDMV, St. Hyacinthe, Quebec, Canada). The Macro-Illumination imaging system (Lighttools, Encinitas, CA) was used to monitor EGFP expression in organs (46). All animal experiments were approved by the Institutional Animal Care and Use Committee of the Experimental Biology Centre of the INRS-Institut Armand-Frappier.

Lymphocyte proliferation assay and quantification of cell-associated viremia. A small amount of heparinized whole blood was used directly for a white blood cell (WBC) count (Unopette; BD Biosciences, Mississauga, Ontario, Canada), and plasma and PBMC were isolated using Ficoll (GE Healthcare, Baie d'Urfé, Quebec, Canada) gradient centrifugation. The proliferation activity was determined using the 5-bromo-2'-deoxyuridine (BrdU) cell proliferation assay (Roche Diagnostics, Laval, Quebec, Canada) according to the manufacturer's instructions. Briefly, the PBMC isolated from each animal were split into two duplicates and either stimulated with 100 μ g/ml phytohemagglutinin (PHA; Sigma, Oakville, Ontario, Canada) or left untreated. The next day, BrdU was added to a final concentration of 10 μ M, and cells were incubated for another 24 h before

they were transferred into black 96-well plates, washed, and fixed at 65°C for 1 h. BrdU incorporation was detected using a peroxidase-linked anti-BrdU antibody and revealed with a chemiluminescent substrate. The signal was detected using a microplate luminescence counter (Luminoskan Ascent, Thermo Electron Corp., Calgary, Alberta, Canada). The proliferation activity was expressed as a ratio between stimulated and nonstimulated cells, allowing for comparison of samples that differ in absolute cell numbers due to the virus-induced leukopenia.

The erythrocytes in EDTA-treated blood were lysed in ACK lysis buffer (150 mM NH₄Cl, 10 mM KHCO₃, 0.01 mM EDTA, pH 7.2 to 7.4), and the isolated PBMC were washed once with phosphate-buffered saline (PBS) solution (Invitrogen, Burlington, Ontario, Canada) and counted. To quantify the cell-associated viremia, quadruplicates of a 10-fold serial dilution of the isolated PBMC were transferred onto VerodogSLAMtag cells seeded in 96-well plates and cultivated for 4 days. The cell-associated virus titer was expressed as TCID₅₀ per 10^6 cells.

Antibodies and staining reagents. Infected T cells were identified immunohistochemically using a mouse anti-CD3 antibody, infected endothelial cells using a mouse anti-von Willebrand factor, and infected glial cells using a rabbit anti-glial fibrillary acidic protein antiserum (all DAKO Cytomation, Mississauga, Ontario, Canada). These antibodies recognize a conserved epitope and have been reported to cross-react with the respective ferret cell type. Neurons were detected using NeuroTrace 530/615 (Invitrogen, Burlington, Ontario, Canada), a red fluorescent variant of the Nissl stain. To visualize all cells present in the field of view, either the nuclear stain 4',6-diamidino-2-phenylindole (DAPI) or the actin stain Alexa Fluor 568-phalloidin was used (both Invitrogen, Burlington, Ontario, Canada).

Staining of tissue sections and microscopic analysis. Animals were euthanized with an overdose of pentobarbital (CDMV, St. Hyacinthe, Quebec, Canada) intraperitoneally. Once a deep plane of anesthesia was reached, each animal was perfused first with 160 ml PBS, followed by 80 ml of 4% paraformaldehyde (PFA). Tissues were harvested, fixed in 4% PFA for at least 24 h at 4°C, and stored in PBS. Prior to sectioning, samples were placed in 30% sucrose in PBS overnight at 4°C, immersed in tissue embedding compound (Triangle Biomedical Sciences, Durham, NC), and frozen on dry ice for at least 1 h. Serial 10- to 15- μ m sections were cut using a cryostat (Kryostat 1720 digital; Leitz, Midland, Ontario, Canada) and mounted on Superfrost Plus slides (Fisher Scientific, Whitby, Ontario, Canada), air dried, and stored at -20°C.

For immunostaining, sections were thawed for 15 min, blocked for 30 min using normal horse serum (Invitrogen, Burlington, Ontario, Canada) diluted to 1/100 in PBS, and incubated with the respective primary antibody for 60 to 90 min at room temperature. After a 1-h incubation with the appropriate Alexa Fluor 568-conjugated secondary antibody (Invitrogen, Burlington, Ontario, Canada), coverslips were mounted in Prolong Gold antifade reagent (Invitrogen, Burlington, Ontario, Canada) and left to harden overnight at 4°C. Fluorescent images were captured using either a standard fluorescent microscope or the confocal laser microscope (MRC 1000; Bio-Rad, Mississauga, Ontario, Canada).

For hematoxylin-and-eosin staining, slides were fixed in 100% MeOH and rehydrated prior to staining for 5 min in Harris' hematoxylin solution (EMD Industries, Gibbstown, NJ). Sections were rinsed in double-distilled H₂O, dipped in an ammonia solution, and counterstained with acidified eosin Y (Sigma-Aldrich, Oakville, Ontario, Canada). Slides were dehydrated, mounted in Entellan mounting medium (EMD Industries, Gibbstown, NJ), and air dried overnight.

RESULTS

A75/17 and its EGFP-expressing derivative A75eH are highly neurovirulent in ferrets. To characterize the mechanism underlying morbillivirus neurovirulence, we chose CDV strain A75/17. This virus has been primarily characterized in dogs, where it causes acute disease including neurological signs in 10% of infected animals (38). In the more sensitive ferret model, rash signifying the onset of the symptomatic disease phase started around 10 days postinoculation (d.p.i.) with the nonrecombinant virus (Fig. 1B, A75/17). All animals subsequently developed severe generalized rash, increasing signs of gastrointestinal and respiratory involvement, and ultimately circling behavior and seizures suggestive of CNS involvement,

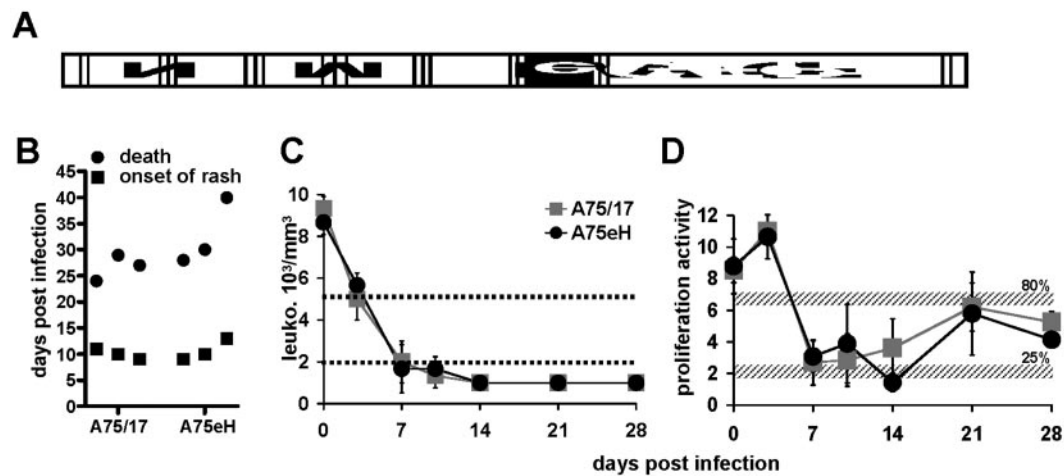


FIG. 1. Comparison of the pathogenicity of the parental CDV strain A75/17 and its EGFP expression recombinant derivative A75eH. (A) Scheme of the A75eH genome with the EGFP open reading frame introduced as an additional transcription unit between the hemagglutinin (H) and polymerase (L) genes. The genome is shown as a white elongated box. The genes are indicated by the letters N (nucleocapsid), P (phosphoprotein), M (matrix), F (fusion), H, and L. The additional EGFP-containing transcription unit is represented by a black box and is marked "eGFP." (B) Time course of infection of groups of three animals. Each pair of symbols represents one animal. Squares indicate the onset of rash, and circles indicate the time of euthanasia for humane reasons. (C) Leukocyte number and (D) in vitro proliferation activity of lymphocytes from these animals. The group ($n = 3$) infected with A75/17 is represented by gray squares, and the group ($n = 3$) infected with A75eH is represented by black circles. Days postinfection are indicated on the x axis, and leukocyte number (leuko.) or proliferation activity is indicated on the y axis. Dotted lines or broad hatched gray lines indicate threshold levels used for the classification as moderate or severe immunosuppression, respectively.

leading to their sacrifice for humane reasons within 3 to 5 weeks after infection (Fig. 1B, A75/17). To produce an infectious cDNA of this strain and eventually insert a reporter gene for easy monitoring of the infection, we cloned and sequenced the viral genome. We confirmed the consensus sequence deposited in GenBank with the accession

no. AF164967. We then assembled an infectious clone based on this consensus sequence and introduced EGFP in an additional transcription unit between the H and L genes (Fig. 1A), to directly visualize infected cells and document viral spread as described previously (46). The corresponding recombinant virus, named A75eH, elicited equivalent courses of disease (Fig.

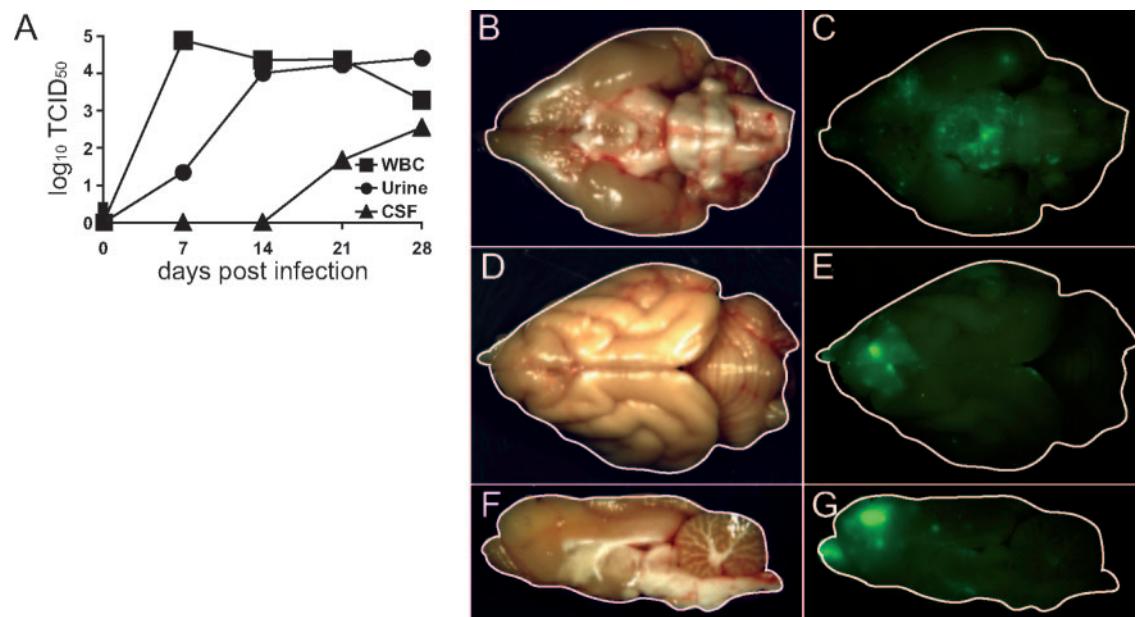


FIG. 2. Replication of CDV in different body fluids and the brain. (A) Number of CDV-infected cells or infectious units in PBMC, urine, and CSF. The cell associated virus titer in the PBMC is expressed as TCID₅₀ per million cells, and the cell-free virus titer in urine and CSF is expressed as TCID₅₀ per ml. (B to G) Visualization of infection in the brain at the end stage of the disease. (B and C) Ventral view of the brain by (B) normal light or (C) EGFP fluorescence excitation. Contours are outlined with a white line. (D and E) Dorsal views of the same sample. (F and G) Sagittal cut separating the left and right hemispheres.

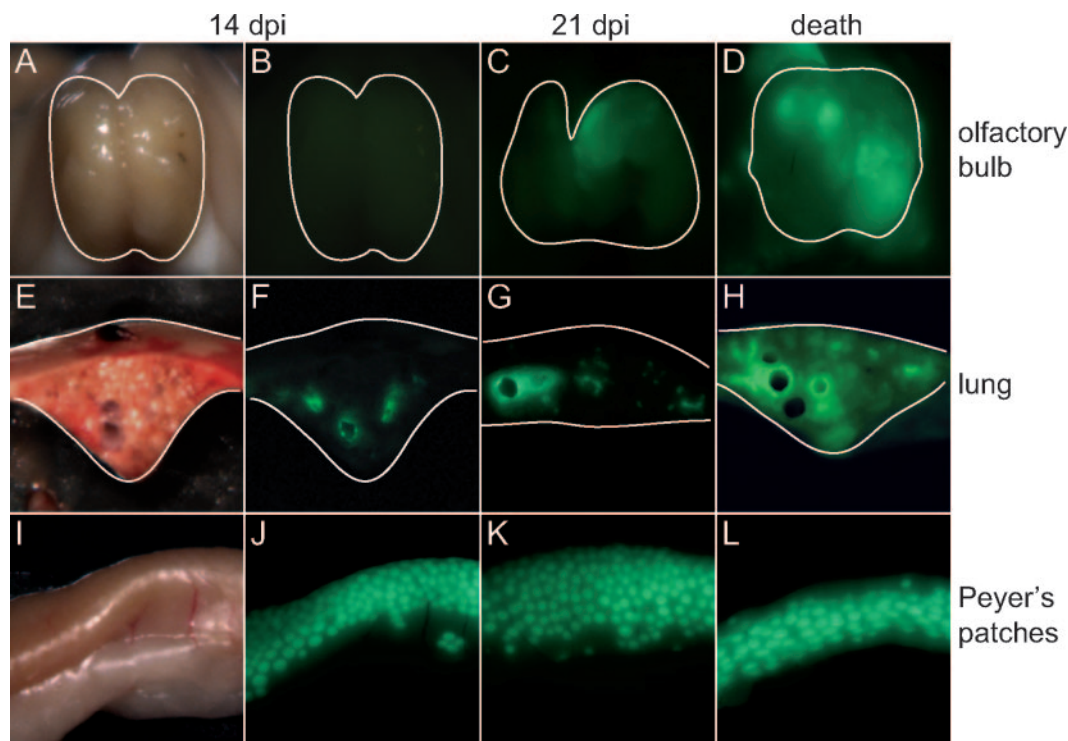


FIG. 3. Time course of CDV dissemination in different tissues. Shown are a macroscopic visualization of infection in the olfactory bulb (A to D), a transverse section of a lung lobe (E to H), and Peyer's patches (panels I to L). The contours of the organs are outlined by a white line. (A, E, and I) Normal light photographs of the different tissues from an animal sacrificed at 14 d.p.i. (B, F, and J) Same organs and time point as above but photographed after EGFP fluorescence excitation. Also shown are the same organs as above from an animal sacrificed at 21 d.p.i. (C, G, and K) and at the time of euthanasia (D, H, and L), photographed after EGFP fluorescence excitation.

1B, A75eH, right side), indicating that EGFP gene addition had no attenuating effect. Animals infected with either virus experienced a 90% loss of WBC in the peripheral blood within the first week after infection (Fig. 1C) and were unable to mount a neutralizing antibody response (data not shown). However, after an initial dramatic drop, the remaining lymphocytes recovered some of their ability to proliferate in response to nonspecific PHA stimulation (Fig. 1D), correlating with the prolonged survival compared to animals infected with the previously used CDV strain 5804P, which succumb to the disease after 14 days (47).

A75eH causes CNS infection. To determine how the observed neurological signs were related to infection, we measured virus titer in WBC, urine, and CSF. Cell-associated virus titers in WBC peaked at 7 d.p.i., followed by a slight drop towards the end of the infection (Fig. 2A). Cell-free virus was detected in the urine 7 d.p.i., reaching values similar to those found in the WBC 14 d.p.i., which correlated with the extensive spread to epithelia throughout the body during the second week of the infection (Fig. 2A). In the CSF, cell-free virus was first detected at 21 d.p.i. and increased steadily until the death of the animal, indicating a substantial infection in CNS areas with contact with the CSF (Fig. 2A).

Macroscopic examination of a brain at the time of euthanasia revealed multiple EGFP-expressing foci in the brain stem (Fig. 2B and C) and the surface of the frontal lobes adjacent to the olfactory bulb (Fig. 2D and E). The median section revealed strong EGFP expression throughout the olfactory bulb

and within the frontal lobes (Fig. 2F and G), while the more caudal parts of the cerebrum and the cerebellum were negative (Fig. 2E and G). This pattern was observed in all animals sacrificed at the end stage of the disease. However, the extent of the spread correlated with the duration of the infection in the respective animal; with those surviving for 35 to 40 days displaying the most widespread EGFP expression, while positive foci were mainly found in the olfactory bulb and adjacent cerebrum in those that had to be sacrificed earlier.

Infection of the CNS occurs after spread to epithelia. We have previously shown that lymphatic organs are the primary targets during the early stages of CDV spread followed by a widespread infection of epithelia throughout the body that coincides with the onset of rash, fever, and gastrointestinal and respiratory signs (46). To determine the timing of CNS invasion, we sacrificed two to three animals at weekly intervals and visualized the extent of infection in Peyer's patches as representative of the lymphatic organs, lung for epithelial tissues, and olfactory bulb as a possible point of CNS entry. The intensity of EGFP expression in Peyer's patches reached its maximum after 1 week (data not shown) and maintained this level throughout the course of the infection (Fig. 3I to L). Again in accordance with our previous findings, we detected EGFP expression in the lung 1 week after inoculation, which was initially limited to the larger bronchi (Fig. 3E and F) and subsequently became increasingly generalized (Fig. 3G and H). The earliest green foci in the olfactory bulb were revealed 21 d.p.i. (Fig. 3A to C). At that time, no EGFP signal was found in

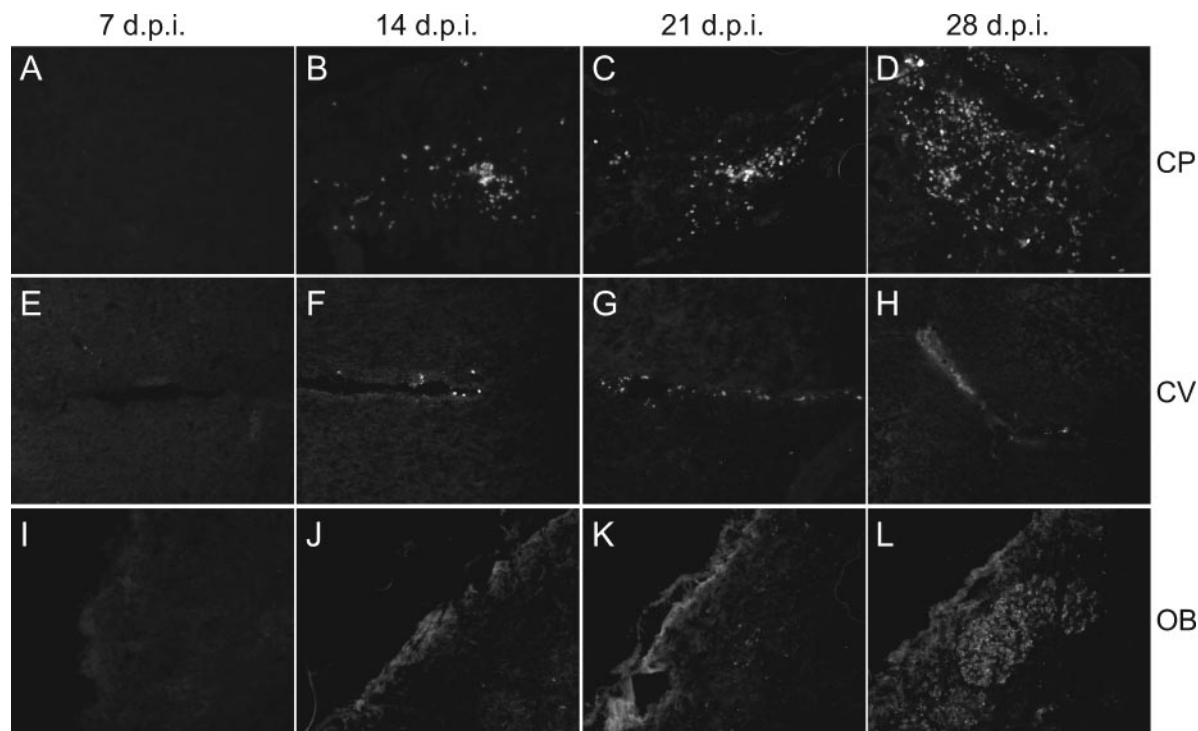


FIG. 4. Time course of CDV dissemination in the CNS. After macroscopic imaging, PFA-perfused brains were fixed in 4% PFA at 4°C for an additional 48 h and transferred into 30% sucrose in PBS at 4°C overnight. Four- to 7-mm-thick sagittal sections were then immersed in tissue embedding compound and frozen on dry ice. Ten- to 15- μ m cryosections were subsequently analyzed for EGFP expression at a 200-fold magnification. Positive cells were mainly detected in the choroid plexus (CP; panels A to D), along cerebral blood vessels (CV; panels E to H), and in the olfactory bulb (OB; panels I to L). Representative regions from animals sacrificed at 7 d.p.i. (A, E, and I), 14 d.p.i. (B, F, and J), 21 d.p.i. (C, G, and K), and 28 d.p.i. (D, H, and L) are shown.

other regions of the brain, further suggesting that the olfactory bulb is an important port of entry. A consecutive increase in EGFP expression in the olfactory bulb and spread to adjacent parts of the CNS were observed in animals sacrificed at or after 28 d.p.i. (Fig. 3D).

CDV accesses the brain through different pathways. While our macroscopic analysis highlighted the importance of the olfactory bulb, previous studies with CDV and MV have identified the choroid plexus and cerebral blood vessels as likely origins of morbillivirus neuroinvasion (11, 39). To analyze the involvement of these structures during different disease stages, we examined sagittal cryosections of the CNS for sites of EGFP expression. Consistent with our macroscopic findings, only single green cells with the round morphology typical of circulating lymphocytes were seen sporadically in the choroid plexus and in the lumen of capillaries at the onset of clinical signs around 7 d.p.i. (data not shown). However, the overall fluorescence did not exceed background levels seen in noninfected controls (Fig. 4A, E, and I), indicating that the intranasal inoculation did not lead to a direct infection of olfactory neurons. After 2 weeks, coinciding with a high-titer cell-associated viremia (Fig. 2A) and the spread to epithelia (Fig. 3F), infected cells were found in the choroid plexus (Fig. 4B) and the vicinity of cerebral blood vessels (Fig. 4F). The first EGFP-positive olfactory nerve fibers were also detected at this time (Fig. 4J), concomitantly with a massive infection of the respiratory mucosa (Fig. 3F). These findings suggest that the infec-

tion of the brain requires prolonged exposure to infected cells, regardless of the point of entry.

At 21 d.p.i., when the first macroscopic signal was detected in the olfactory bulb (Fig. 3C), a majority of olfactory nerve fibers were infected and spread into the olfactory glomeruli was observed (Fig. 4K). The simultaneous increase of EGFP-expressing cells associated with the choroid plexus and blood vessels (Fig. 4C and G) coincided with the detection of free virus in the CSF (Fig. 2A). Within the subsequent weeks, the number of infected cells at the different entry points increased continuously (Fig. 4D, H, and L). In addition, there was evidence of virus spread to the lining of the ventricles, the pia mater, and the underlying molecular layer of the cerebral and cerebellar cortex via the CSF (Fig. 5A and B), invasion of the brain parenchyma surrounding blood vessels indicative of direct hematogenous dissemination (Fig. 5C), and migration from the olfactory glomeruli to mitral cells and further towards the olfactory cortex (Fig. 5D). The only histopathological change consistently observed in all animals, was a lymphocyte infiltration in the choroid plexus starting at 14 d.p.i. and persisting until the time of death (Fig. 5E). The brain parenchyma (Fig. 5F) and olfactory bulb (not shown) rarely showed signs of inflammation, most likely due to the severe leukopenia and immunosuppression at this time.

Extensive hematogenous infection of glial cells and neurons is a late event. To identify the target cells over the course of the infection, we stained consecutive sagittal sections with markers

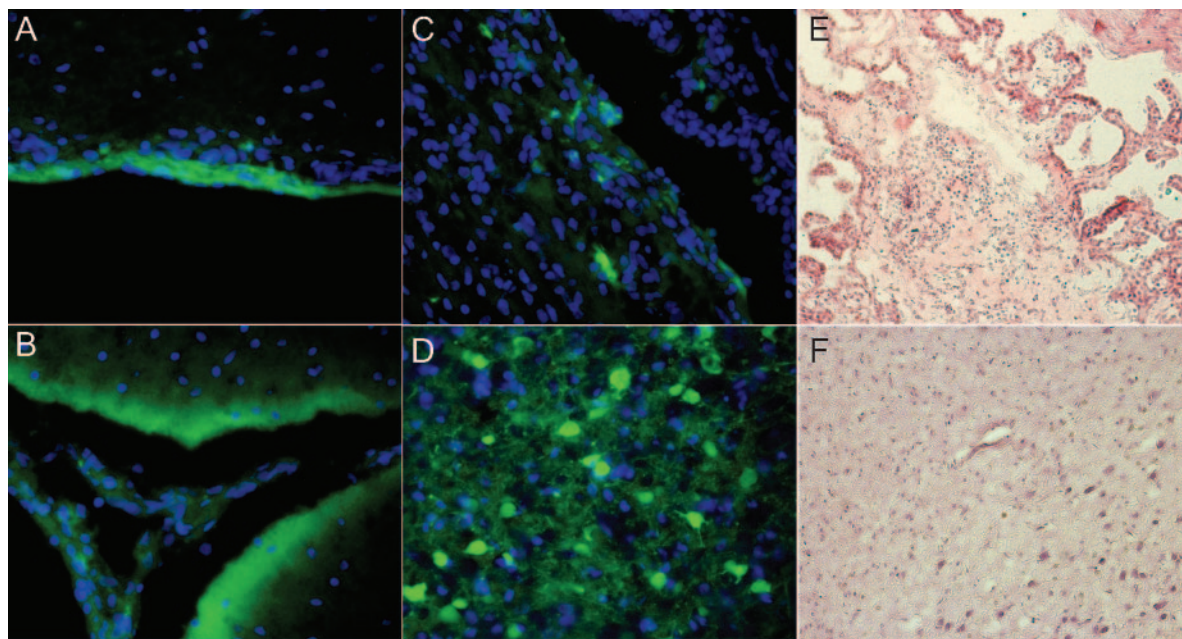


FIG. 5. CDV spread and histopathological changes in the CNS at advanced disease stages. Shown is microscopic analysis of cryosections stained blue with DAPI to visualize cell nuclei at a 400-fold magnification (A to D) or stained with hematoxylin and eosin at a 200-fold magnification (E and F). (A) Pia mater, (B) parenchyma bordering a blood vessel in the cerebellum, (C) ependyma bordering a ventricle, and (D) olfactory bulb. (E) Choroid plexus and (F) parenchyma of the frontal lobe from an animal sacrificed at 28 d.p.i.

specific for the different cell types present in the brain. Up to 21 d.p.i., the EGFP-expressing cells detected in the choroid plexus and those with a round morphology found in the vicinity of blood vessels were mostly T cells (Fig. 6A, E, and I). Occasionally, infected monocytes or B cells were also found in these locations (data not shown), consistent with the high-level viremia (Fig. 2A, squares). Capillary endothelial cells were the only infected nonimmune cells associated with hematogenous spread consistently detected between 14 and 21 d.p.i. (Fig. 6B, F, and J). Once the virus had gained access to the ventricles and pia mater via the CSF around 28 d.p.i., glial cells were the dominating infected cell type (Fig. 6C, G, and K). At this time, the first EGFP-positive neurons were also observed: mostly in close proximity to infected glial cells (Fig. 6D, H, and L). Consistent with CSF-mediated dissemination, infected epithelial cells were detected in the dura mater and the choroid plexus (data not shown).

The olfactory bulb is a main point of CDV CNS entry. In contrast to many other respiratory viruses with neurovirulent potential (2, 4), direct CNS entry via the olfactory bulb was not considered a major infection route for morbilliviruses. However, in our study, olfactory nerves were infected as early as 14 d.p.i. (Fig. 4J), and the olfactory bulb was the first location of macroscopic EGFP expression (Fig. 3C). We were able to follow this CNS invasion pathway microscopically from the neurons located in the olfactory mucosa, along the olfactory nerve filaments passing through the cribriform plate, and into the olfactory glomeruli, which constitute the synapse between olfactory nerve fibers and mitral cells.

At 14 d.p.i., infected cells were detected throughout the olfactory mucosa in cryosections stained with the neuronal cell body-specific Nissl stain (Fig. 7A, yellow cells), indicating that

these cells were infected at the same time as the surrounding mucosal epithelial cells. The green staining seen at the rostral margin of the olfactory bulb at this time (Fig. 4J) represents multiple individual olfactory nerve filaments (Fig. 7B, counterstained with an actin marker). The detection of infected mitral cells as early as 21 d.p.i. (Fig. 7C, green cell, counterstained with an actin marker) indicates that the virus is transmitted across neuronal synapses and thus has the potential to spread anterogradely to deeper CNS structures.

DISCUSSION

Neurovirulent distemper in ferrets and dogs. Ferrets are exquisitely sensitive to CDV and usually succumb to the infection without ever developing an effective immune response (47). Taking advantage of EGFP-expressing 5804P-derived viruses, we previously demonstrated massive infection of lymphatic organs and the resulting dramatic depletion of circulating lymphocytes during the initial disease phases. At 7 d.p.i., most of the remaining circulating lymphocytes are infected, setting the stage for the invasion of epithelial tissues, including the upper and lower respiratory tract (46). Here we operated with the neurovirulent strain A75eH, which does not kill infected animals within 2 weeks and therefore allows us to monitor subsequent disease phases, including neuroinvasion. We report the detection of first positive cells in the CNS around 2 weeks p.i., coinciding with widespread epithelial infection. This timing indicates that CNS invasion occurs only after extensive spread through lymphatic and epithelial tissues rather than directly as a consequence of the intranasal route of infection as has been reported for primary neurotropic viruses (28). The localization of infected cells in the olfactory nerves, the cho-

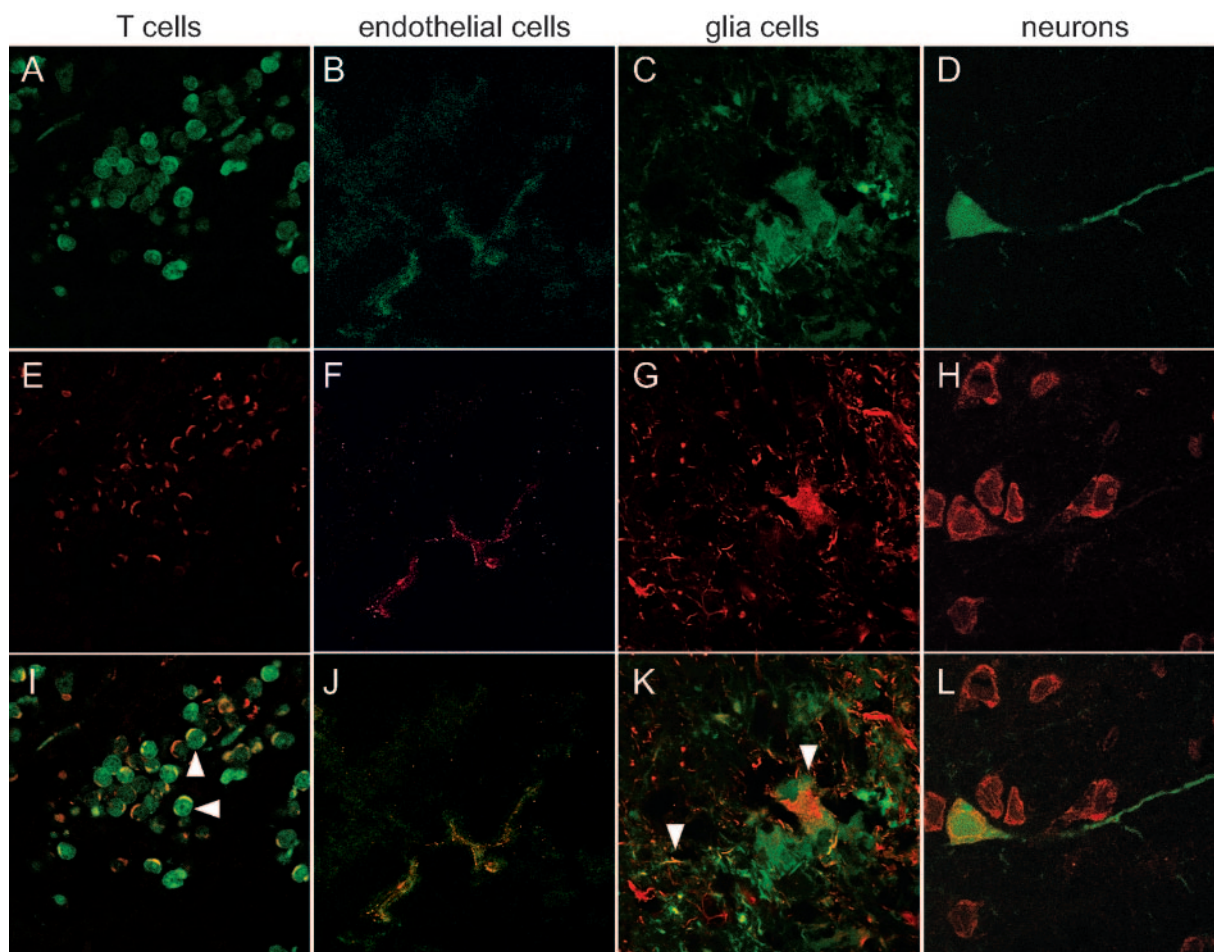


FIG. 6. Identification of cells infected through hematogenous spread. Shown is confocal microscopic analysis of cryosections stained with antibodies against different cellular markers at a 1,000-fold magnification. (A to D) CDV-infected cells; (E to H) respective cellular markers, visualized with an Alexa Fluor 568-labeled secondary antibody; and (I to L) composite image of the two colors. (A, E, and I) Infected T cells in the choroid plexus and (B, F, and J) endothelial cells in a cerebral capillary at 14 d.p.i. identified with a mouse anti-CD3 or anti-von Willebrand factor antibody, respectively. (C, G, and K) Infected glial cells and (D, H, and L) neurons at 28 d.p.i. visualized with a rabbit anti-glial fibrillary acidic protein polyclonal antiserum or the 530/615 NeuroTrace Nissl stain, respectively. Examples of double-positive cells are indicated by white triangles. The partial overlap of red and green signals seen in some cases is due to the fact that most of the antibodies recognize proteins located in the cell membrane while EGFP is expressed in the cytoplasm.

roid plexus, and the vicinity of blood vessels furthermore reflects two distinct routes of invasion: anterogradely via the olfactory nerves and hematogenously through infected circulating lymphocytes.

The course of CDV in dogs initially follows the same pattern, including the infection of cells in locations consistent with hematogenous invasion (31). However, neutralizing antibodies are detected in up to 90% of the animals 2 to 3 weeks p.i., indicating the onset of an effective antiviral immune response that controls and then eliminates the infection and coincides with resolution of the disease signs (31, 39, 41). In the CNS, an inflammatory process characterized by lymphocyte invasion is observed, which results in a chronic demyelinating disease in 10 to 30% of the animals (52). In ferrets and the subset of dogs that fail to mount an immune response, the virus continues its spread through the brain, ultimately establishing a widespread infection of different CNS cell types (39, 45). In ferrets, we observed that this spread occurs, depending on the port of

entry, either from the outer layers into the parenchyma or anterogradely from the olfactory nerve through the mitral cells further along the olfactory signaling route. Given the other similarities in the course of disease in ferrets and dogs, entry through the olfactory bulb may occur in dogs as well.

CDV neurovirulence in ferrets as morbillivirus neuroinvasion model. The incidence of CNS invasion associated with morbillivirus infection varies among the different family members. CDV and the viruses that infect marine mammals frequently cause CNS complications, while rinderpest and peste des petits ruminants viruses generally do not affect the brain (7). Measles virus holds an intermediate position, as it causes several distinct but relatively rare CNS diseases. Among those, postinfectious encephalomyelitis occurs in 1 in 1,000 cases within weeks of acute measles, but the extent of viral replication seems minor and the pathology is immune mediated (14, 32). On the other hand, extensive viral replication was documented in the context of a rare fatal course of the acute disease

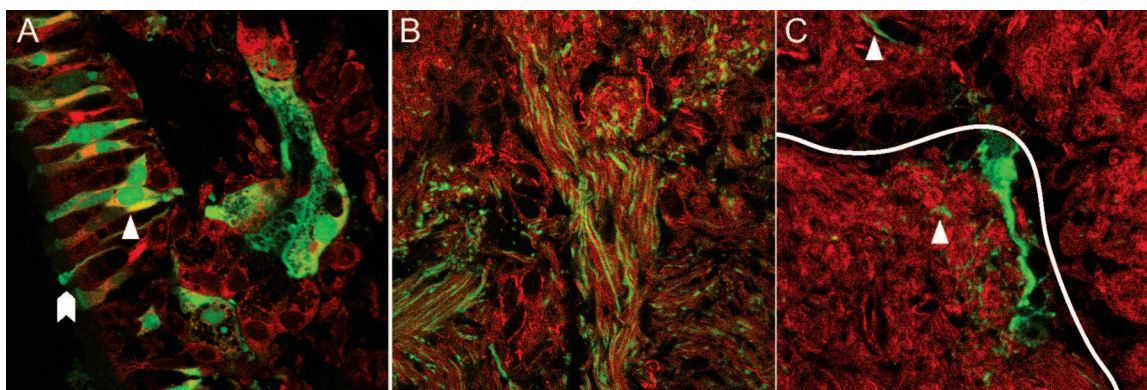


FIG. 7. Visualization of CNS invasion via the olfactory route. Shown is confocal microscopic analysis of cryosections at 1,000-fold magnification. (A) Merged image of the olfactory mucosa at 14 d.p.i. stained with the 530/615 NeuroTrace Nissl stain to visualize neuronal cell bodies. The triangle indicates an infected olfactory receptor neuron, and the arrowhead marks a sensory cilium protruding into the mucus layer. (B and C) Merged images of (B) the olfactory nerve filaments at 14 d.p.i. and (C) the olfactory glomeruli at 21 d.p.i. stained with Alexa Fluor 568-phalloidin to visualize actin in the surrounding structures. An individual olfactory glomerulum is located in the lower left corner of panel C, indicated by a white line. Examples of individual nerve fibers are highlighted by white triangles.

(24, 30), and two chronic manifestations, measles inclusion body encephalitis and subacute sclerosing panencephalitis (SSPE) (5). The former occurs between 2 and 6 months after acute infection and is limited to individuals with an innate immune defect resulting in an inability to clear the virus during acute infection and subsequent persistence in the CNS (16, 32). A similar disease form, known as old dog encephalitis, is also observed for CDV, where it occurs more frequently (3). All chronic manifestations of morbillivirus CNS infections are inevitably fatal and characterized by massive and widespread infection of neurons (25).

While the significance of our observations for the pathogenic mechanisms underlying SSPE and old dog encephalitis remains to be explored, hematogenous invasion has been deduced from histological analysis of brain sections of measles patients who died from acute encephalitis and the histopathological analyses of marine mammals that succumbed to morbillivirus infections (9, 11, 21, 30). In addition, the dissemination pattern documented in the later infection stages in ferrets strongly resembles that of fatal measles in individuals that are unable to combat the infection (13, 24). This link between the extent of spread and the ability of the host's immune response to control the infection is also apparent in studies in immunocompetent and immunosuppressed mice (26, 42). In summary, our findings suggest that CDV neuroinvasion in ferrets reflects the events occurring in the context of other morbillivirus infections.

Mechanisms of CNS entry by *Paramyxoviridae*. This study shows remarkable parallels between CDV entry into the CNS of ferrets and the mechanisms of brain invasion by other *Paramyxoviridae*. Several paramyxoviruses with neurovirulent potential, including morbilliviruses, mumps virus, and Newcastle disease virus, efficiently infect circulating lymphocytes, resulting in a cell-associated viremia that lasts throughout the symptomatic disease phase (32, 34, 50). This provides ample opportunity for infected lymphocytes to traffic through the blood-brain and blood-choroid plexus barrier and locally release virus, starting infection of resident epithelial and endothelial cells (12, 15). Consistent with this hematogenous route

of CNS invasion, infected cells are usually first detected in the choroid plexus and in close association with cerebral blood vessels (34, 39). Once inside the CSF, the viruses may invade the different membranes surrounding the CNS, the ependyma, and the superficial lining of the cerebral cortex (34, 49), followed by infection of neurons and glia cells in close proximity and subsequent spread into deeper layers (19, 26, 29). Taken together, these observations suggest that paramyxoviruses use classical hematogenous CNS invasion pathways described for several other neurotropic viruses (17, 33).

In addition to hematogenous CNS invasion, entry via the olfactory bulb has been demonstrated for Sendai, La Piedad Michoacan, and, more recently, Nipah viruses, all of which also cause massive respiratory epithelial infection (1, 27, 49). In the olfactory mucosa, which lines the roof of the nasal cavity, the dendrites of mature olfactory receptor neurons and these respiratory epithelial cells reside in close proximity, and easy virus transition between the different cell types is conceivable. Since the axons of the bipolar olfactory receptor neurons enter the olfactory bulb by passing through the cribriform plate, these neurons, once infected, provide direct access to the CNS. The axons synapse in the olfactory glomeruli with the dendrites of mitral cells, the corresponding second order neurons, which in turn project further to the deeper olfactory and limbic systems, thus providing a rapid way of accessing these regions for viruses capable of crossing the synaptic space (35). This pathway is used by various neurotropic viruses (28), and the capacity to move transcellularly across either dendrodendritic or axonal synapses has been identified as an important neurovirulence determinant (43). Our findings add to the mounting evidence that entry via the olfactory bulb and spread along the olfactory signaling route are common among paramyxoviruses and should be considered alongside the classical hematogenous entry pathway.

ACKNOWLEDGMENTS

We thank Marcel Desrosiers for excellent support with the confocal microscopy and Brian Ward and Christoph Springfield for comments

on the manuscript. We are thankful to all laboratory members for support and lively discussions.

This work was supported by a grant from the CIHR (MOP-66989) to V.V.M. and a scholarship from the Fondation Armand-Frappier to P.A.R.

REFERENCES

- Allan, G. M., F. McNeilly, I. Walker, T. Linne, J. Moreno-Lopez, P. Hernandez, S. Kennedy, B. P. Carroll, B. Herron, J. C. Foster, and B. Adair. 1996. A sequential study of experimental porcine paramyxovirus (LPMV) infection of pigs: immunostaining of cryostat sections and virus isolation. *J. Vet. Diagn. Investig.* **8**:405–413.
- Aronsson, F., B. Robertson, H. G. Ljunggren, and K. Kristensson. 2003. Invasion and persistence of the neuroadapted influenza virus A/WSN/33 in the mouse olfactory system. *Viral Immunol.* **16**:415–423.
- Axthelm, M. K., and S. Krakowka. 1998. Experimental old dog encephalitis (ODE) in a gnotobiotic dog. *Vet. Pathol.* **35**:527–534.
- Barnett, E. M., M. D. Cassell, and S. Perlman. 1993. Two neurotropic viruses, herpes simplex virus type 1 and mouse hepatitis virus, spread along different neural pathways from the main olfactory bulb. *Neuroscience* **57**: 1007–1025.
- Cattaneo, R., A. Schmid, D. Eschle, K. Baczko, V. ter Meulen, and M. A. Billeter. 1988. Biased hypermutation and other genetic changes in defective measles viruses in human brain infections. *Cell* **55**:255–265.
- Cocks, B. G., C. C. Chang, J. M. Carballido, H. Yssel, J. E. de Vries, and G. Aversa. 1995. A novel receptor involved in T-cell activation. *Nature* **376**:260–263.
- Cosby, S. L., W. P. Duprex, L. A. Hamill, M. Ludlow, and S. McQuaid. 2002. Approaches in the understanding of morbillivirus neurovirulence. *J. Neurovirol.* **8**(Suppl. 2):85–90.
- Domingo, M., L. Ferrer, M. Pumarola, A. Marco, J. Plana, S. Kennedy, M. McAliskey, and B. K. Rima. 1990. Morbillivirus in dolphins. *Nature* **348**:21.
- Domingo, M., J. Visa, M. Pumarola, A. J. Marco, L. Ferrer, R. Rabanal, and S. Kennedy. 1992. Pathologic and immunocytochemical studies of morbillivirus infection in striped dolphins (*Stenella coeruleoalba*). *Vet. Pathol.* **29**: 1–10.
- Duprex, W. P., I. Duffy, S. McQuaid, L. Hamill, S. L. Cosby, M. A. Billeter, J. Schneider-Schaulies, V. ter Meulen, and B. K. Rima. 1999. The H gene of rodent brain-adapted measles virus confers neurovirulence to the Edmonston vaccine strain. *J. Virol.* **73**:6916–6922.
- Esolen, L. M., K. Takahashi, R. T. Johnson, A. Vaisberg, T. R. Moench, S. L. Wesselingh, and D. E. Griffin. 1995. Brain endothelial cell infection in children with acute fatal measles. *J. Clin. Investig.* **96**:2478–2481.
- Frisk, A. L., M. König, A. Moritz, and W. Baumgärtner. 1999. Detection of canine distemper virus nucleoprotein RNA by reverse transcription-PCR using serum, whole blood, and cerebrospinal fluid from dogs with distemper. *J. Clin. Microbiol.* **37**:3634–3643.
- Gazzola, P., L. Cocito, E. Capello, L. Roccatagliata, M. Canepa, and G. L. Mancardi. 1999. Subacute measles encephalitis in a young man immunosuppressed for ankylosing spondylitis. *Neurology* **52**:1074–1077.
- Gendelman, H. E., J. S. Wolinsky, R. T. Johnson, N. J. Pressman, G. H. Pezeshkpour, and G. F. Boisset. 1984. Measles encephalomyelitis: lack of evidence of viral invasion of the central nervous system and quantitative study of the nature of demyelination. *Ann. Neurol.* **15**:353–360.
- Goh, K. J., C. T. Tan, N. K. Chew, P. S. Tan, A. Kamarulzaman, S. A. Sarji, K. T. Wong, B. J. Abdullah, K. B. Chua, and S. K. Lam. 2000. Clinical features of Nipah virus encephalitis among pig farmers in Malaysia. *N. Engl. J. Med.* **342**:1229–1235.
- Griffin, D. E. 2001. Measles virus, p. 1401–1441. *In* D. M. Knipe and P. M. Howley (ed.), *Fields virology*, 4th ed., vol. 1. Lippincott Williams & Wilkins, Philadelphia, Pa.
- Griffin, D. E., A. P. Byrnes, and S. H. Cook. 2004. Emergence and virulence of encephalitogenic arboviruses. *Arch. Virol. Suppl.* **2004**:21–33.
- Griot, C., M. Vandevelde, M. Schobesberger, and A. Zurbriggen. 2003. Canine distemper, a re-emerging morbillivirus with complex neuropathogenic mechanisms. *Anim. Health Res. Rev.* **4**:1–10.
- Higgins, R. J., S. G. Krakowka, A. E. Metzler, and A. Koestner. 1982. Primary demyelination in experimental canine distemper virus induced encephalomyelitis in gnotobiotic dogs. Sequential immunologic and morphologic findings. *Acta Neuropathol. (Berlin)* **58**:1–8.
- Kennedy, S. 1998. Morbillivirus infections in aquatic mammals. *J. Comp. Pathol.* **119**:201–225.
- Kennedy, S., J. A. Smyth, P. F. Cush, P. Duignan, M. Platten, S. J. McCullough, and G. M. Allan. 1989. Histopathologic and immunocytochemical studies of distemper in seals. *Vet. Pathol.* **26**:97–103.
- Liebert, U. G., and V. ter Meulen. 1987. Virological aspects of measles virus-induced encephalomyelitis in Lewis and BN rats. *J. Gen. Virol.* **68**: 1715–1722.
- Lisiak, J. A., and M. Vandevelde. 1979. Polioencephalomalacia associated with canine distemper virus infection. *Vet. Pathol.* **16**:650–660.
- McQuaid, S., S. L. Cosby, K. Koffi, M. Honde, J. Kirk, and S. B. Lucas. 1998. Distribution of measles virus in the central nervous system of HIV-seropositive children. *Acta Neuropathol. (Berlin)* **96**:637–642.
- McQuaid, S., J. Kirk, A. L. Zhou, and I. V. Allen. 1993. Measles virus infection of cells in perivascular infiltrates in the brain in subacute sclerosing panencephalitis: confirmation by non-radioactive in situ hybridization, immunocytochemistry and electron microscopy. *Acta Neuropathol. (Berlin)* **85**:154–158.
- Miyamae, T. 2005. Differential invasion by Sendai virus of abdominal parenchymal organs and brain tissues in cortisone- and cyclophosphamide-based immunosuppressed mice. *J. Vet. Med. Sci.* **67**:369–377.
- Mori, I., T. Komatsu, K. Takeuchi, K. Nakakuki, M. Sudo, and Y. Kimura. 1995. Parainfluenza virus type 1 infects olfactory neurons and establishes long-term persistence in the nerve tissue. *J. Gen. Virol.* **76**:1251–1254.
- Mori, I., Y. Nishiyama, T. Yokochi, and Y. Kimura. 2005. Olfactory transmission of neurotropic viruses. *J. Neurovirol.* **11**:129–137.
- Parede, L., and P. L. Young. 1990. The pathogenesis of velogenic Newcastle disease virus infection of chickens of different ages and different levels of immunity. *Avian Dis.* **34**:803–808.
- Plaza, J. A., and G. J. Nuovo. 2005. Histologic and molecular correlates of fatal measles infection in children. *Diagn. Mol. Pathol.* **14**:97–102.
- Rima, B. K., N. Duffy, W. J. Mitchell, B. A. Summers, and M. J. Appel. 1991. Correlation between humoral immune responses and presence of virus in the CNS in dogs experimentally infected with canine distemper virus. *Arch. Virol.* **121**:1–8.
- Rima, B. K., and W. P. Duprex. 2006. Morbilliviruses and human disease. *J. Pathol.* **208**:199–214.
- Ryan, G., T. Grimes, B. Brankin, M. J. Mabruk, M. J. Hosie, O. Jarrett, and J. J. Callanan. 2005. Neuropathology associated with feline immunodeficiency virus infection highlights prominent lymphocyte trafficking through both the blood-brain and blood-choroid plexus barriers. *J. Neurovirol.* **11**: 337–345.
- Saika, S., M. Kidokoro, T. Ohkawa, A. Aoki, and K. Suzuki. 2002. Pathogenicity of mumps virus in the marmoset. *J. Med. Virol.* **66**:115–122.
- Shepherd, G., and C. A. Greer. 1990. Olfactory bulb, p. 133–169. *In* G. M. Shepherd (ed.), *Synaptic organization of the brain*. Oxford University Press, Oxford, United Kingdom.
- Sidorenko, S. P., and E. A. Clark. 2003. The dual-function CD150 receptor subfamily: the viral attraction. *Nat. Immunol.* **4**:19–24.
- Stephensen, C. B., J. Welter, S. R. Thaker, J. Taylor, J. Tartaglia, and E. Paoletti. 1997. Canine distemper virus (CDV) infection of ferrets as a model for testing *Morbillivirus* vaccine strategies: NYVAC- and ALVAC-based CDV recombinants protect against symptomatic infection. *J. Virol.* **71**:1506–1513.
- Summers, B. A., H. A. Greisen, and M. J. Appel. 1984. Canine distemper encephalomyelitis: variation with virus strain. *J. Comp. Pathol.* **94**:65–75.
- Summers, B. A., H. A. Greisen, and M. J. Appel. 1979. Early events in canine distemper demyelinating encephalomyelitis. *Acta Neuropathol. (Berlin)* **46**: 1–10.
- Tatsuo, H., N. Ono, and Y. Yanagi. 2001. Morbilliviruses use signaling lymphocyte activation molecules (CD150) as cellular receptors. *J. Virol.* **75**: 5842–5850.
- Tipold, A., P. Moore, A. Zurbriggen, I. Burgener, G. Barben, and M. Vandevelde. 1999. Early T cell response in the central nervous system in canine distemper virus infection. *Acta Neuropathol. (Berlin)* **97**:45–56.
- Urbanska, E. M., B. J. Chambers, H. G. Ljunggren, E. Norrby, and K. Kristensson. 1997. Spread of measles virus through axonal pathways into limbic structures in the brain of TAP1 $-/-$ mice. *J. Med. Virol.* **52**:362–369.
- van den Pol, A. N., K. P. Dalton, and J. K. Rose. 2002. Relative neurotropism of a recombinant rhabdovirus expressing a green fluorescent envelope glycoprotein. *J. Virol.* **76**:1309–1327.
- Vandevelde, M., and A. Zurbriggen. 2005. Demyelination in canine distemper virus infection: a review. *Acta Neuropathol. (Berlin)* **109**:56–68.
- Vandevelde, M., A. Zurbriggen, R. J. Higgins, and D. Palmer. 1985. Spread and distribution of viral antigen in nervous canine distemper. *Acta Neuropathol. (Berlin)* **67**:211–218.
- von Messling, V., D. Milosevic, and R. Cattaneo. 2004. Tropism illuminated: lymphocyte-based pathways blazed by lethal morbilliviruses through the host immune system. *Proc. Natl. Acad. Sci. USA* **101**:14216–14221.
- von Messling, V., C. Springfield, P. Devaux, and R. Cattaneo. 2003. A ferret model of canine distemper virus virulence and immunosuppression. *J. Virol.* **77**:12579–12591.
- von Messling, V., G. Zimmer, G. Herrler, L. Haas, and R. Cattaneo. 2001. The hemagglutinin of canine distemper virus determines tropism and cytopathogenicity. *J. Virol.* **75**:6418–6427.
- Weingartl, H., S. Czub, J. Copps, Y. Berhane, D. Middleton, P. Marszal, J. Gren, G. Smith, S. Ganske, L. Manning, and M. Czup. 2005. Invasion of the central nervous system in a porcine host by Nipah virus. *J. Virol.* **79**:7528–7534.
- Wilczynski, S. P., M. L. Cook, and J. G. Stevens. 1977. Newcastle disease as

- a model for paramyxovirus-induced neurologic syndromes. II. Detailed characterization of the encephalitis. *Am. J. Pathol.* **89**:649–666.
51. **Winters, K. A., L. E. Mathes, S. Krakowka, and R. G. Olsen.** 1983. Immunoglobulin class response to canine distemper virus in gnotobiotic dogs. *Vet. Immunol. Immunopathol.* **5**:209–215.
52. **Wunschmann, A., S. Alldinger, E. Kremmer, and W. Baumgartner.** 1999. Identification of CD4⁺ and CD8⁺ T cell subsets and B cells in the brain of dogs with spontaneous acute, subacute-, and chronic-demyelinating distemper encephalitis. *Vet. Immunol. Immunopathol.* **67**:101–116.
53. **Zhu, Y. D., J. Heath, J. Collins, T. Greene, L. Antipa, P. Rota, W. Bellini, and M. McChesney.** 1997. Experimental measles. II. Infection and immunity in the rhesus macaque. *Virology* **233**:85–92.